Enhanced photocatalytic efficiency of layered CdS/CdSe heterostructures: Insights from first principles electronic structure calculations

Sulakshana Shenoy and Kartick Tarafder[1]

Department of Physics, National Institute of Technology, Srinivasnagar, Surathkal, Mangalore
Karnataka-575025, India

E-mail: karticktarafder@gmail.com

Abstract

Metal sulfides are emerging as an important class of materials for photocatalytic applications, because of their high photo responsive nature in the wide visible light range. In this class of materials, CdS with a direct band gap of 2.4 eV, has gained special attention due to the relative position of its conduction band minimum, which is very close to the energies of the reduced protons. However, the photogenerated holes in the valence band of CdS are prone to oxidation and destroy its structure during photocatalysis. Thus constructing a CdS based heterostructure would be an effective strategy for improving the photocatalytic performance. In this work we have done a detail theoretical investigation based on hybrid density functional theory calculation to get insight into the energy band structure, mobility and charge transfer across the CdS/CdSe heterojunction. The results indicate that CdS/CdSe forms type-II heterostructure that has several advantages in improving the photocatalytic efficiency under visible light irradiation.

Keywords: heterostructure, photocatalysis, electronic structure, band alignment, density functional theory

(Some figures may appear in colour only in the online journal)

1. Introduction

The field of processing semiconductor-based photocatalysts has expanded rapidly in the last four decades. Notable developments have already been achieved especially in the area of organic pollutants decomposition and water splitting [1–7]. Most of the significant developments in this area are mainly based on titanium dioxide (TiO_2), which exhibits strong redox potential and excellent photocatalytic activity. However, a wide band gap of 3.2 eV in this material hinders its applicability as it can only be driven through UV light radiation which is only 3% of solar spectrum [5, 8–14]. Therefore designing and investigation of efficient visible light responsive materials for photocatalytic activity has attracted researcher with a

considerable attention from the viewpoint of cost, availability and environmental friendliness [15–20]. Few good visible light responsive semiconductor photocatalysts have recently been reported [15, 16], among them cadmium sulfide (CdS) turns out to be very effective because of its relatively low band gap of 2.4 eV. CdS belongs to II–VI group semiconductors, shows broad absorbance in the visible light region. Also its relatively negative conduction band position with respect to water reduction potential make this material suitable for water spitting [21–23]. Efficient generation of charge carriers, charge separation and migration to the catalytic surface are the determining factors that affects the photocatalytic performance of a given semiconductor [24]. In photocatalytic reaction such as water splitting or photo-degradation of organic pollutants, the redox reactions on the semiconductor's

---

[1] Author to whom any correspondence should be addressed.

surface must be thermodynamically favorable. A photocat-alytic reaction can only take place when the band edges of semiconductor are appropriately placed relative to the redox reaction potentials. In particular, the position of the valence band maximum (VBM) and conduction band minimum (CBM) must lie lower and higher in energy relative to the oxi-dation and reduction potentials respectively. In case of CdS, the photogenerated electrons in the conduction band have a good reducing ability for hydrogen evolution. However the photogenerated holes in the valence band are prone to self-oxidation, results to severe photocorrosion in the system that significantly reduces its photocatalytic efficiency. To over-come this drawback, suitable band engineering is very essen-tial which in turn help to separate the electron–hole pairs generated under visible light irradiation, decrease the rate of recombination and photocorrosion. For example, excitation in a semiconductor which is in contact with a second semi-conductor with relatively low conduction band minimum will result electron transport into the second material. Furthermore, if the valence band maximum of second material is higher in energy than that of first semiconductor, the hole transport to the first material will occur. In either of the cases, the composite material is referred to as type-II heterostructure. Heterostruc-ture formation of CdS with some other efficient photocatalyst could be a suitable strategy for further improvement of the photocatalytic efficiency and its durability. Cadmium selenide (CdSe) is one among the many other narrow band gap semi-conductors having a direct band gap of 1.7 eV, capable of absorbing more of visible light spectrum, would be a good choice for making the heterostructure [25, 26]. Experimental studies shows that combination of CdS/CdSe heterostructure could be a suitable candidate for water splitting and photo-voltaic applications, owing to its internal charge separation at the interface [26, 27]. Although an extensive experimental investigation have been carried out for CdS/CdSe heterostruc-tures towards its photocatalytic applications, proper theoreti-cal knowledge such as the detail electronic structure, accurate position and character of the band edges are still lacking, which are very essential for a better understanding of catalytic mech-anism such as light induced charge separation, electron and hole pair recombination etc. In this work, we have used hybrid density functional theory calculations to obtain an accurate electronic band structure of CdS(110) and CdSe(110) surfaces as well as CdS/CdSe heterojunction and subsequently investi-gated the possible improvement of photocatalytic activity with the help of their proper band alignment with respect to the reduction and oxidation potential.

2. Computational method

We employed density functional theory calculation using the projector augment wave (PAW) method implemented in Vienna *ab initio* simulation package (VASP) to deter-mine the accurate geometric and electronic structure of the CdS, CdSe surfaces and CdS/CdSe heterostructure [28–30]. We adopted the generalized gradient approximation (GGA) of Perdew–Burke–Ernzerhof (PBE) scheme to describe the exchange and correlation potential, and used the empirical
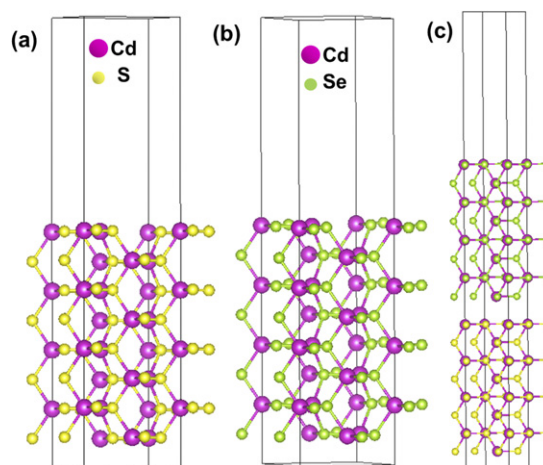

Figure 1. Optimized geometric structures of (a) CdS(110) surface, (b) CdSe(110) surface and (c) CdS/CdSe heterostructure. Here pink, yellow and green spheres represents Cd, S and Se atoms respectively.

correction method proposed by Drimme (DFT-D3), which was proved to be a good description for long range vdW interactions, to depict vdW interaction. A very high wave func-tion cutoff energy of 500 eV was used in each calculation to obtain accurate result. The structure relaxation was per-formed in each case setting the convergence criteria 1×10^{-5} eV for energy and 0.01 eV Å^{-1} for force. Since PBE functional underestimates the band-gap due to the presence of artificial self-interaction, we performed hybrid-DFT calculation using Heyd–Scuseria–Ernzerhof (HSE06) hybrid functional, with 25% Hartree–Fock exchange energy contribution to accurately determine the band-edge positions [31].

3. Results and discussion

Before exploring the properties of CdS/CdSe heterostructure, we first investigated the crystal structure of their bulk counter-parts. Both CdS and CdSe belong to cubic sphalerite structure with $F-43m$ space group. The optimized lattice parameters $a = b = c = 5.82$ Å for CdS and $a = b = c = 6.07$ Å for CdSe are in good agreement with the experimental values [32]. Next we modeled CdS(110) and CdSe(110) surface, using optimized bulk geometry. A vacuum region of 10 Å thickness perpen-dicular to the surface is used in the unit cell, to avoid the interactions between neighboring slabs. The unit cell of an eight layer CdS(110) and CdSe(110) slabs are illustrated in figures 1(a) and (b). Finally the heterojunction was modeled by placing CdSe(110) slab over CdS(110) as shown in figure 1(c) considering an average values for in-plane lattice parameters, with a lattice mismatch less than 2.0%. We further relaxed all the atoms in the modeled surfaces and heterostructures to get the appropriate electronic structure information. We observed that the optimum separation between the surfaces is 4.74 Å is little higher than the inter layer distances of CdS(110) and CdSe(110) which are 4.11 Å and 4.15 Å respectively.

The bulk CdS and bulk CdSe are direct band gap semi-conductors in which both the VBM and CBM are located at
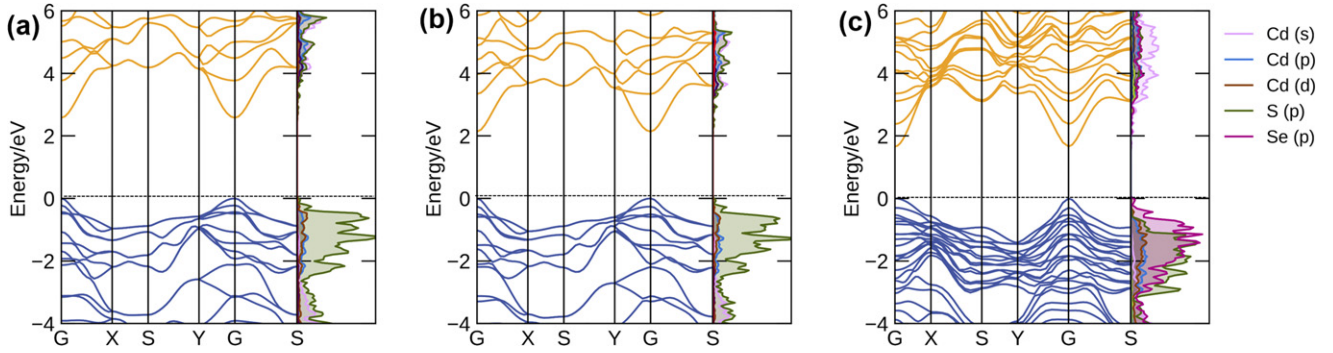
Figure 2. Calculated band structures and atom projected density of state plots of (a) CdS(110) surface (b) CdSe(110) surface and (c) CdS/CdSe heterostructure using hybrid-DFT calculation.

Γ point. The calculated band gaps are 2.37 eV and 1.80 eV respectively, which are consistent with the values reported in the literature [33]. In case of CdS(110) and CdSe(110) surfaces, we found both the surfaces have direct band gap of 2.58 eV and 2.14 eV respectively at the Γ point. Our calculation shows that the CdS/CdSe heterostructure is also a direct gap system with band gap 1.66 eV at Γ point. Band structures of CdS(110), CdSe(110) and the CdS/CdSe heterostructure are shown in figures 2(a)–(c). To understand the orbital character of band edges, we have plotted the atom projected DOS for each system as shown in figures 2(a)–(c)). From the atom projected DOS of CdS(110), it is evident that the VBM consists of S 3p states, whereas Cd 3d states are contributed to the CBM. In case of CdSe(110) surface, Se 4p is contributing to the VBM, whereas Cd 4p states are contributing to the CBM. In CdS/CdSe heterojunction, VBM is dominated by S 3s and Se 4p states whereas CBM is composed of Cd 3d character. In order to investigate the catalytic activity of this materials, the relative band position of the heterostructure with respect to the reduction and oxidation potential of water is very essential.

The work function (Φ) of material, in this case is a crucial parameter, commonly used as an intrinsic reference for band alignment [34]. This is the minimum energy required for an electron to reach vacuum level from Fermi level (E_F). One can estimate material specific work function from the following equation:

$$\Phi = E_{vac} - E_F \tag{1}$$

where E_F is the Fermi energy. E_{vac} is the energy of stationary electron in the vacuum nearby the surface. This can be estimated from the average electrostatic potential plot for a surface calculation, considering sufficient amount of vacuum in the unit cell. Calculated electrostatic potential for CdS(110), CdSe(110) and CdS/CdSe heterostructure are plotted in figures 3(a)–(c). On the basis of equation (1), our calculated work functions for CdS(110), CdSe(110) and CdS/CdSe heterostructure are 4.99 eV, 4.60 eV and 4.72 eV respectively.

The redox potential of a semiconductor is assessed by the positions of its valence and conduction band edges with respect to the normal hydrogen electrode (NHE) potential. Generally, a positive valence band maximum of a semiconductor with

respect to the NHE potential indicates that the photogenerated holes have stronger oxidation ability, while the negative conduction band minimum with respect to the NHE potential shows a strong reducing ability of the photogenerated electrons. Therefore accurate band edge position with respect to NHE will provide detail information about the photocatalytic efficiency of a semiconductor. We have obtained the edge positions of VB and CB for all three systems considering the Mulliken electronegativity rules [34], where the energetic position of the CBM and VBM is determined through following equations:

$$E_{VB} = \chi - E_e + \frac{1}{2}E_g \tag{2}$$

$$E_{CB} = E_{VB} - E_g \tag{3}$$

Here E_g represents the band gap of the system, E_e is the energy of free electrons in the hydrogen scale (4.5 eV), E_{VB} and E_{CB} are the VB and CB edge potentials, respectively [35, 36]. χ in equation (2) is the Mulliken electronegativity of the semiconductor which can be obtained by taking the geometric mean of the Mulliken electronegativity of constituent atoms in the semiconductor. The χ of an atom is the arithmetic mean of its electron affinity and the first ionization energy. The calculated values of χ for CdS and CdSe are 5.18 and 5.14 eV respectively. Using our calculated band gap values for CdS(110) and CdSe(110) along with equations (2) and (3), we have obtained the band edge positions of CB and VB of CdS with respect to NHE as -0.62 V and 1.96 V respectively and the band edge positions of CB and VB of CdSe are -0.43 V and 1.71 V respectively. The results are illustrated in figure 4.

In the case of CdS/CdSe heterostructure, the relative positions of CB and VB of both the semiconductors are expected to be changed significantly because of the change in the Fermi energy. Since the work function of CdS (4.99 eV) is higher than CdSe (4.60 eV), electrons will flow from CdSe to CdS while forming the heterojunction, until the Fermi level of both the semiconductors are aligned. Our calculation shows that the work function of the CdS/CdSe heterojunction is 4.72 eV, which is lying in between that of their individual semiconductors. Therefore, at equilibrium the CB and VB of CdS shift upwards by 0.49 eV, while CB and VB of CdSe shifted
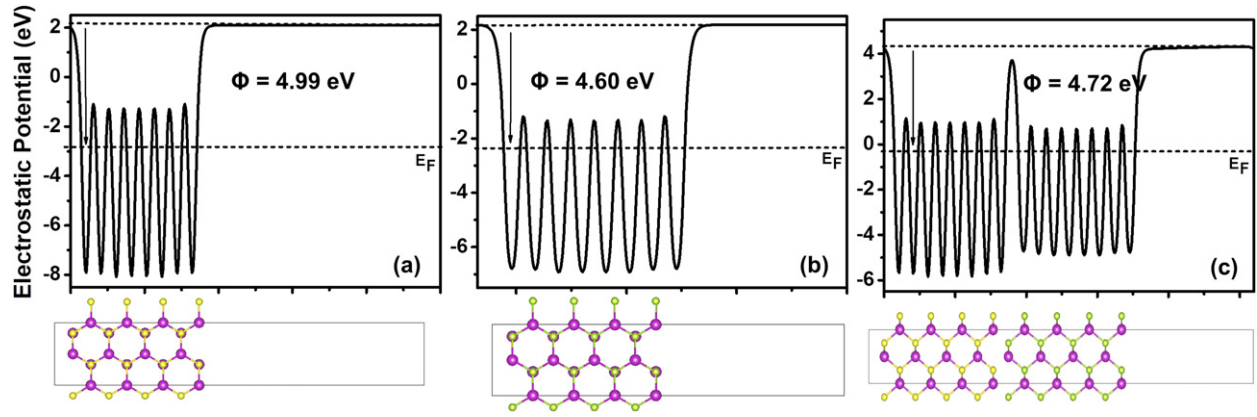
Figure 3. Average electrostatic potential plots for (a) CdS(110) surface, (b) CdSe(110) surface and (c) CdS/CdSe heterostructure. Calculated work functions for CdS(110), CdSe(110) and CdS/CdSe heterostructure are 4.99 eV, 4.60 eV and 4.72 eV respectively.
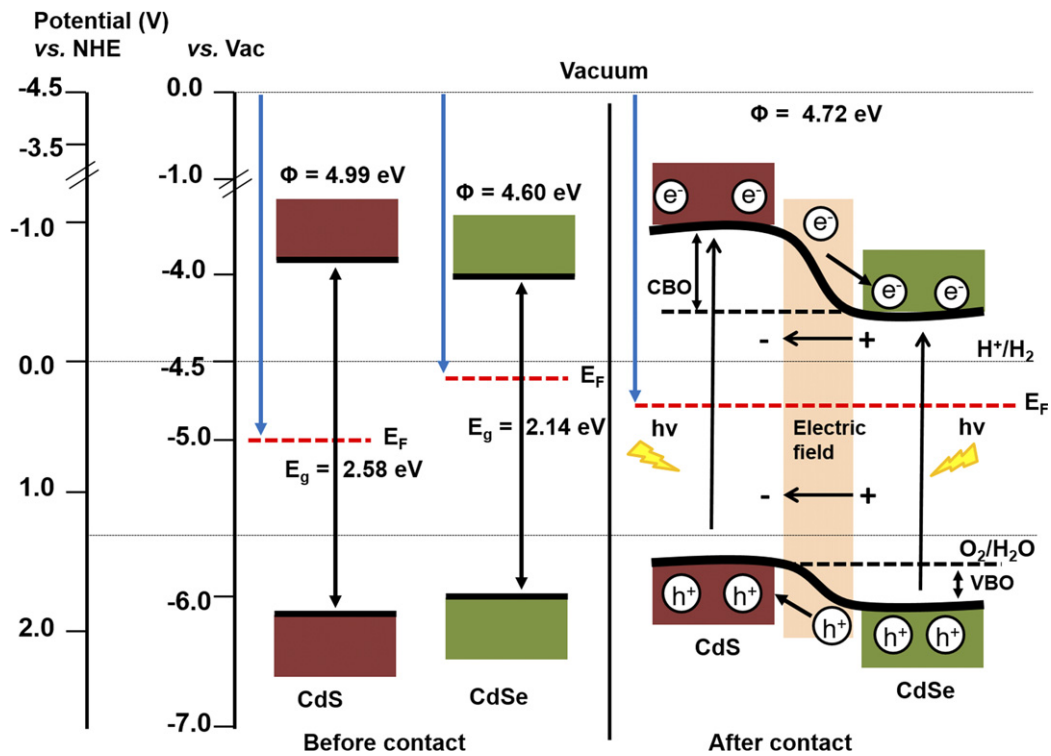

Figure 4. Diagram of band edge positions of CdS(110) and CdSe(110) surfaces before and after the formation of heterojunction with respect to the vacuum level.

downwards by 0.1 eV due to the change of Fermi level in the heterojunction. This led to the generation of large band offset both in valence band and conduction band. An internal charge separation is expected due to this band offsets.

To confirm the charge separation at the interface of CdS/CdSe heterojunction, we have calculated the charge density difference using the following equation

$$\Delta \rho = \rho_{CdS/CdSe} - \rho_{CdS}(110) - \rho_{CdSe}(110) \qquad (4)$$

here $\rho_{CdS/CdSe}$, $\rho_{CdS}(110)$ and $\rho_{CdSe}(110)$ represent the charge densities of CdS/CdSe heterostructure, the CdS(110) and the CdSe(110) surfaces respectively. The result shown in figure 5(b), clearly indicates that the charge density is

redistributed by the formation of hole-rich and electron-rich regions near the semiconductor interface. The accumulation of electrons in CdS is indicated by yellow isosurface, and electron depletion in the CdSe side is shown as cyan iso-surface in figure 5(a). Note that the charge redistribution is confined in a small region close to the CdS/CdSe interface. There is no significant change is visible in the region far-ther away from the interface. This is because of the strong build up potential due to the separated charges, which acts against the diffusion process of the separated electron/holes. The planar-averaged electron density difference along the z-direction for the heterojunction is plotted in the figure 5(a) indicates that the edge of CdS in the junction is populated with
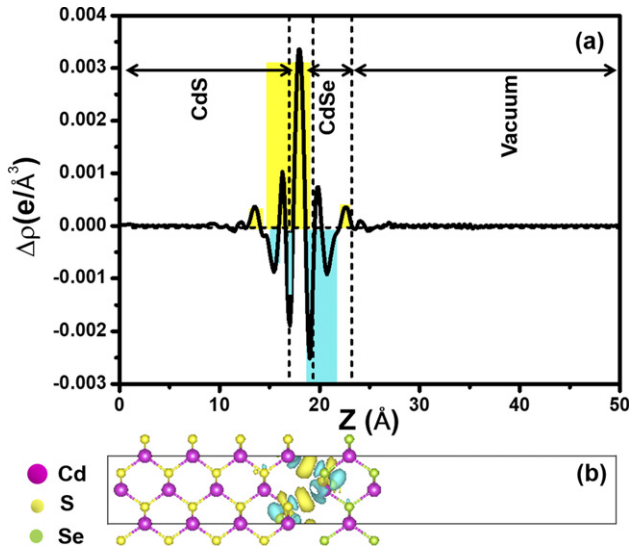
Figure 5. (a) Planar-averaged electron density difference $\Delta\rho(z)$ for CdS/CdSe heterostructure. The cyan and yellow region represents electron depletion and electron accumulation respectively. (b) Charge density difference plot for CdS/CdSe heterostructure.

Table 1. Effective mass of charge carriers in CdS(110) surface, CdSe(110) surface and CdS/CdSe heterostructure.

System	m_e^* (in e-mass)	m_h^* (in e-mass)	m_h^*/m_e^*
CdS(110)	0.272	−1.183	4.349
CdSe(110)	0.223	−1.060	4.75
CdS/CdSe heterostructure	0.210	−1.230	5.857

negative charge carrier, while CdSe edge is composed of positive charge carrier. This signifies that the charge separation leads to the formation of built-in electric field at the interface in the direction from CdSe to CdS during formation of CdS/CdSe heterojunction which will help to separate the photogenerated charge carriers spatially across the heterojunction in opposite direction, thereby enhancing the possibility of higher photocatalytic performance.

The calculated values of valence band offset (VBO) and conduction band offset (CBO) for CdS/CdSe heterostructure are 0.14 eV and 0.58 eV respectively. Under visible light irradiation, when the electron transition takes place from the VB to the CB of the heterostructure, owing to the existence of CBO, the electrons will start moving from CdS to CdSe. On the other hand, the VBO induces simultaneous movement of holes created in the VB from CdSe to CdS. As a result, negative charges get accumulated over CdSe and conversely positive charges on CdS. Thus, photoexcited electrons and holes are effectively separated and will participate in the photocatalytic reaction. The photoexcited electrons of the CdS/CdSe heterosructure accumulated in the CB which is mainly contributed from CdSe. Since the CB edge potential is −0.53 V with respect to NHE, which is more negative than that of H^+/H_2O (0 V), has ability to reduce the H^+ to H_2; while the photogenerated holes accumulated at VB which is from CdS portion of the heterojunction has edge potential of 1.61 V with respect to NHE, is more positive than that of O_2/H_2O (1.23 V), has very good oxidation ability to produce super-oxide anion radicals and degrade the organic pollutants. Therefore, CdS/CdSe becomes a type II heterojunction in which band edge positions are favorable for simultaneous oxidation and reduction reactions.

The mobility of charge carriers in a semiconductor photocatalyst has a greater influence on its photocatalytic activity. Higher the mobility better is the performance of the photocatalyst. The mobility of charge carrier can be estimated from the

band effective masses of a semiconductor as the mobility of the charge carriers is inversely proportional to the effective mass. Therefore a lower value of effective mass promotes efficient migration of charge carriers and suppresses their recombination rate. We have estimated the effective masses of electrons and holes by fitting the parabolic portions to the CBM and VBM using the following equation:

$$m_x^* = \hbar^2 \left(\frac{d^2 E}{dk^2} \right)^{-1} \tag{5}$$

where $m_x^*(x = e, h)$ represents effective mass of x-type charge carrier, E is the band edge energy as a function of the wave vector k and $\hbar$ is the reduced Planck constant. A large difference in m_e^* and m_h^* i.e. larger value of m_h^*/m_e^* in a semiconductor will suppress the charge carrier recombination [37]. Calculated effective masses are tabulated in table 1. Interestingly, our calculation shows that value of m_h^*/m_e^* is greater in heterostructure than that of individual semiconductor counterpart, indicating a larger lifetime of photogenerated charge carriers in the heterostructure that will further improve the photocatalytic activity.

4. Conclusion

In summary, the electronic structures of the CdS(110), CdSe(110) and CdS/CdSe heterostructure were investigated on the basis of hybrid-DFT method. Calculated band structure and atom projected DOS confirm that the CdS/CdSe forms a type-II heterostructure. The proper band edge positions and their alignment with respect to the NHE were determined from the calculated band gap and work function for each surface. The band edge positions of both the semiconductors are changed with the Fermi level while formation of heterostructure and a large band offset both in valence and conduction band was observed. Therefore, under the influence of visible light irradiation, the photogenerated electrons and holes could move from CB of CdS to that of CdSe and from VB of CdSe to that of CdS respectively. The existence of an internal electric field near the interface due to large band offsets will facilitate the charge separation across the CdS/CdSe interface, which in turn reduce the recombination of electron–hole pairs. The charge carrier mobility is also improved in the heterostructure and the band alignment of the system is such that both photo-reduction and photo-oxidation processes associated with water splitting are energetically feasible. The results indicate that the CdS/CdSe heterojunction may have wide application in photocatalysis for pollutant degradation and water splitting.

Finally, our present work not only discloses a promising candidate for photocatalysis, but also provides a new pathway for investigating novel and next generation heterojunctions for their applications in photocatalysis.

Acknowledgment

ORCID iDs

Kartick Tarafder ⬤ https://orcid.org/0000-0002-6299-654X

References

[1] Serpone N and Pelizzetti E 1989 *Photocatalysis: Fundamentals and Applications* (Hoboken, NY: Wiley-Interscience)
[2] Linsebigler A L, Lu G and Yates J T 1995 *Chem. Rev.* **95** 735–58
[3] Hoffmann M R, Martin S T, Choi W and Bahnemann D W 1995 *Chem. Rev.* **95** 69–96
[4] Asahi R, Morikawa T, Ohwaki T, Aoki K and Taga Y 2001 *Science* **293** 269–71
[5] Schneider J, Matsuoka M, Takeuchi M, Zhang J, Horiuchi Y, Anpo M and Bahnemann D W 2014 *Chem. Rev.* **114** 9919–86
[6] Liu J, Wang H and Antonietti M 2016 *Chem. Soc. Rev.* **45** 2308–26
[7] Spasiano D, Marotta R, Malato S, Fernandez-Ibañez P and Di Somma I 2015 *Appl. Catal., B Environ.* **170–171** 90–123
[8] Ola O and Maroto-Valer M M 2015 *J. Photochem. Photobiol. C Photochem. Rev.* **24** 16–42
[9] He Y, Sutton N B, Rijnaarts H H H and Langenhoff A A M 2016 *Appl. Catal., B Environ.* **182** 132–41
[10] Marinho B A, Djellabi R, Cristóvão R O, Loureiro J M, Boaventura R A R, Dias M M, Lopes J C B and Vilar V J P 2017 *Chem. Eng. J.* **318** 76–88
[11] Farner Budarz J, Turolla A, Piasecki A F, Bottero J-Y, Antonelli M and Wiesner M R 2017 *Langmuir* **33** 2770–9
[12] Pueyo N, Miguel N, Mosteo R, Ovelleiro J L and Ormad M P 2017 *J. Environ. Sci. Health, Part* A **52** 182–8
[13] Low J, Cheng B and Yu J 2017 *Appl. Surf. Sci.* **392** 658–86
[14] Liu N, Chen X, Zhang J and Schwank J W 2014 *Catal. Today* **225** 34–51
[15] Schultz D M and Yoon T P 2014 *Science* **343** 1239176
[16] Rao M P, Sathishkumar P, Mangalaraja R V, Asiri A M, Sivashanmugam P and Anandan S 2018 *J. Environ. Chem. Eng.* **6** 2003–10
[17] Low J, Yu J, Jaroniec M, Wageh S and Al-Ghamdi A A 2017 *Adv. Mater.* **29** 1601694
[18] Zhao H, Sun S, Jiang P and Xu Z 2017 *Chem. Eng. J.* **315** 296–303
[19] Zhao H, Sun S, Wu Y, Jiang P, Dong Y and Xu Z 2017 *Carbon* **119** 56–61
[20] Lin F, Shao Z, Li P, Chen Z, Liu X, Li M, Zhang B, Huang J, Zhu G and Dong B 2017 *RSC Adv.* **7** 15053–9
[21] Zhou P, Le Z, Xie Y, Fang J and Xu J 2017 *J. Alloys Compd.* **692** 170–7
[22] Bera R, Kundu S and Patra A 2015 *ACS Appl. Mater. Interfaces* **7** 13251–9
[23] Garg P, Kumar S, Choudhuri I, Mahata A and Pathak B 2016 *J. Phys. Chem* C **120** 7052–60
[24] Cheng L, Xiang Q, Liao Y and Zhang H 2018 *Energy Environ. Sci.* **11** 1362–91
[25] Chauhan H, Kumar Y, Dana J, Satpati B, Ghosh H N and Deka S 2016 *Nanoscale* **8** 15802–12
[26] Bera R, Dutta A, Kundu S, Polshettiwar V and Patra A 2018 *J. Phys. Chem* C **122** 12158–67
[27] Bridewell V L, Alam R, Karwacki C J and Kamat P V 2015 *Chem. Mater.* **27** 5064–71
[28] Kresse G and Furthmüller J 1996 *Comput. Mater. Sci.* **6** 15–50
[29] Blöchl P E 1994 *Phys. Rev.* B **50** 17953–79
[30] Perdew J P and Wang Y 1992 *Phys. Rev.* B **45** 13244–9
[31] Heyd J, Scuseria G E and Ernzerhof M 2003 *J. Chem. Phys.* **118** 8207–15
[32] Wei S-H and Zhang S B 2000 *Phys. Rev.* B **62** 6944–7
[33] Mo Y, Tian G and Tao J 2017 *Chem. Phys. Lett.* **682** 38–42
[34] Liu J 2015 *J. Phys. Chem* C **119** 28417–23
[35] Guo J, Zhou Z, Wang T, Lu Z, Yang Z and Liu C 2017 *Curr. Appl. Phys.* **17** 1714–20
[36] Chen X, Shen S, Guo L and Mao S S 2010 *Chem. Rev.* **110** 6503–70
[37] Li Y, Wu M, Yang D, Zeng H, Zhang T, Shen J, Zhang B and Li Q 2019 *Catalysts* **9** 712